Cancer Research

Bicyclic Peptides as a New Modality for Imaging and Targeting of Proteins Overexpressed by Tumors

Matthias Eder[1,2], Silvia Pavan[3], Ulrike Bauder-Wüst[4], Katerine van Rietschoten[3], Ann-Christin Baranski[1,2], Helen Harrison[3], Spencer Campbell[3], Catherine L. Stace[3], Edward H. Walker[3], Liuhong Chen[3], Gavin Bennett[3], Gemma Mudd[3], Ursula Schierbaum[5], Karin Leotta[5], Uwe Haberkorn[5,6], Klaus Kopka[4], and Daniel P. Teufel[3]

Abstract

Molecular imaging of cancers using probes specific for tumor-associated target proteins offers a powerful solution for providing information regarding selection of targeted therapy, patient stratification, and response to therapy. Here we demonstrate the power of bicyclic peptides as targeting probes, exemplified with the tumor-overexpressed matrix metalloproteinase MT1-MMP as a target. A bicyclic peptide with subnanomolar affinity towards MT1-MMP was identified, and its radioconjugate showed selective tumor uptake in an HT1080 xenograft mouse model. Proteolytic stabilization of the peptide by chemical modification significantly enhanced the *in vivo* tumor signal [from 2.5%ID/g to 12%ID/g at 1 hour post injection (p.i.)]. Studies using mouse xenograft models with different cell lines show a robust correlation between tumor signals and *in vivo* MT1-MMP expression levels. Fatty acid modification of the bicyclic peptide extended its circulating half-life, resulting in increased tumor signals (36%ID/g at 6 hours p.i.). Comparative work with an equipotent radiolabeled MT1-MMP targeting antibody demonstrated starkly differential biodistribution and tumor accumulation properties, with the tumor signal slowly increasing to 6.2%ID/g within 48 hours. The rapid tumor penetration characteristics of bicyclic peptides, coupled with high potency and chemical versatility, thus offer high-contrast imaging probes for clinical diagnostics with compelling additional potential in targeted therapy.

Significance: This work demonstrates the potential of bicyclic peptides as a platform for the development of high-contrast imaging probes for potential use in clinical cancer diagnostics and molecularly targeted therapeutics.

Introduction

In recent decades, the advent of targeted molecular therapies has shown greatly improved patient outcomes in the treatment of certain types of cancer. In contrast to traditional nonspecific cytotoxic chemotherapeutic agents, targeted molecular therapies, such as mAb and tyrosine kinase inhibitors, interfere with specific molecular targets or pathways associated with tumorigenesis (1, 2). Effective molecular diagnosis of tumors informing on antigen expression and consequently the optimal choice of targeted therapy to date mostly relies on biopsies for IHC, FISH, or real-time PCR analyses. Collection of such biopsies are invasive, limited to physically accessible tumor sites, and often do not permit repeated sampling at the same lesion (1, 3, 4). By contrast, molecular imaging by PET or single photon emission computed tomography (SPECT) using tracer molecules selective for tumor antigens enables the noninvasive, holistic visualization of cancerous lesions. Thus, molecular imaging can directly inform the choice of targeted therapy, staging, definition of tumor boundaries for surgical resection, and real-time response during and after therapy.

Imaging agents selective for tumor-associated antigens have been widely studied preclinically, and comprise radiolabeled mAb's, peptides, or small molecules. In principle, peptides offer favorable properties due to rapid tissue and tumor distribution kinetics, good tumor-to-blood (T/B) signal ratio, chemical versatility, comparable ease of manufacture, and low immunogenic potential. However, development of novel peptide-based imaging agents is hampered by difficulties in obtaining high affinity leads that also display high *in vivo* stability to circulating and membrane-bound proteases in the vascular system. Advances in *in vitro* evolution technologies that enable identification of peptides with tailored binding specificities and proteolytic stability enhancing modifications offer the potential for overcoming some of these difficulties in developing peptide-based imaging agents.

Here we for the first time evaluate and demonstrate the potential of bicyclic peptides as a platform for diagnostic

[1]Department of Nuclear Medicine, University Medical Center, Faculty of Medicine, University of Freiburg, Freiburg, Germany. [2]Division of Radiopharmaceutical Development, German Cancer Consortium (DKTK), partner site Freiburg, and German Cancer Research Center (DKFZ), Heidelberg, Germany. [3]Bicycle Therapeutics Limited, Babraham Research Campus, Cambridge, United Kingdom. [4]Division of Radiopharmaceutical Chemistry, German Cancer Research Center (DKFZ), Heidelberg, Germany. [5]Clinical Cooperation Unit Nuclear Medicine, German Cancer Research Center (DKFZ), Heidelberg, Germany. [6]Department of Nuclear Medicine, Heidelberg University Hospital, Heidelberg, Germany.

Note: Supplementary data for this article are available at Cancer Research Online (http://cancerres.aacrjournals.org/).

Corresponding Author: Daniel P. Teufel, Bicycle Therapeutics Limited, Cambridge CB22 3AT, UK. Phone: 00447786865261; E-mail: danteufel@cantab.net

doi: 10.1158/0008-5472.CAN-18-0238

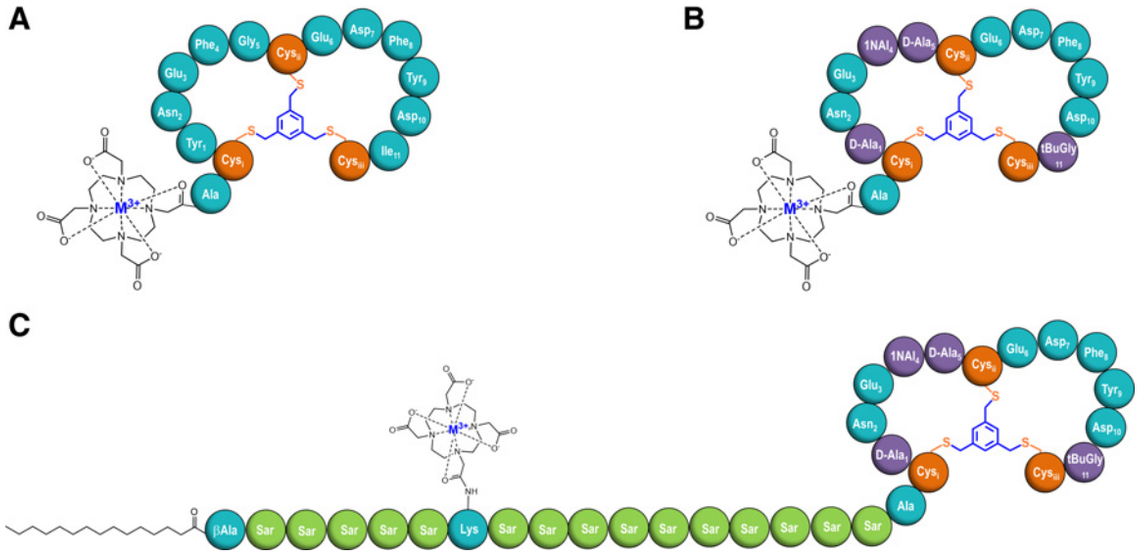

Figure 1.

Diagrammatic structures of key bicyclic peptides. **A,** DOTA-modified BCY-B3. The DOTA-complexed radionuclide is depicted as M^{3+}, with coordination bonds shown through dotted lines. Loop 1 is situated between Cys_i, Cys_{ii}, and Loop 2 between Cys_{ii}, Cys_{iii}. The cysteine-derived thioether bonds connect to the central 1,3,5-trismethylbenzene scaffold, forming the bicyclic peptide structure as shown. Amino acids are described using standard three letter nomenclature, with AA numbering as shown. **B,** Structure of stabilized, DOTA-modified BCY-C2; substituted positions are highlighted in purple. AA abbreviations are provided in the main text. **C,** Structure of palmitoylated, DOTA-modified BCY-D1 containing the extended sarcosine spacer and stabilized peptide sequence.

imaging and targeting. Bicyclic peptides are identified by phage display selections using encoded peptide libraries cyclized with an organochemical scaffold (5). Bicyclic peptides are considered to be more stable to proteases than their linear counterparts, and a large contact surface area with a range of target proteins frequently offers candidate molecules with high affinities and selectivities (6–8).

In this work, we chose the tumor-associated membrane type 1 matrix metalloproteinase MT1-MMP (or MMP-14) as a target due to its overexpression and associated poor prognosis in a variety of cancers (e.g., non–small cell lung cancer, gastric cancer, and breast cancer; refs. 9–11). The clinical interest of MT1-MMP in the treatment of cancer is underscored by the development of an MT1-MMP specific antibody DX-2400, which induced significantly slowed tumor progression and reduced formation of metastatic lesions in mouse xenograft models (12).

Phage selections identified 1.8 kDa bicyclic peptide with high binding affinity and selectivity to MT1-MMP. Using radioconjugates thereof, *in vivo* studies showed high tumor uptake in mouse models, which increased further upon chemical optimization of the peptide's proteolytic stability properties, and upon serum half-life extension through fatty acid conjugation. Thus, the novel bicyclic peptide scaffolds described here (Fig. 1A–C) represent highly attractive entities for diagnostic imaging of cancer-associated target proteins, and hold great promise for theranostic applications in molecular targeted therapy as conjugates with therapeutic radionuclides or cytotoxins.

Materials and Methods

Peptide synthesis

Peptide synthesis was performed by standard Fmoc solid-phase chemistry, and cyclization was performed as previously described (5), with details provided in Supplementary Materials and Methods.

Protein expression and phage selections

Details of protein expression, phage library generation, and selections as previously disclosed (5, 7) are described in Supplementary Materials and Methods.

Affinity determination by fluorescence polarization

The affinities of bicyclic peptides to MT1-MMP were either determined by titration of fluoresceinated peptides with increasing concentrations of PEX, or indirectly by competition of a fluoresceinated peptide:PEX complex with un-labeled bicyclic peptide. Details are described in Supplementary Materials and Methods.

Quantitative plasma stability measurements

Peptide stock solutions (200 μmol/L in DMSO) were mixed with human or mouse plasma (Seralabs) to a final concentration of 4 μmol/L, and incubated at 37°C up to 24 hours. Forty microliters of samples were taken and stored at −80°C. For LC/MS analysis, defrosted samples were mixed with 120 μL of 1:3:3 (v/v/v) water/acetonitrile/methanol. Suspensions were centrifuged 40 minutes (4°C, 13,000 rpm), and supernatants quantitated by LC/MS-MS using a Waters Xevo TQ-D instrument, comparing signals against a standard curve of the same peptides. Half-lives (except BCY-B5) were reported as >>48 hours due to absence of significant degradation over 24 hours (Supplementary Table S1).

Pharmacokinetics of BCY-B2

BCY-B2 was dosed to one group of 12 male CD1 mice as a single intravenous, 5.925 mg/kg dose using a 1.19 mg/mL solution

prepared from DMSO peptide stocks diluted 1:20 in PBS. Blood samples were taken from two animals per time-point, at 0.08, 0.5, 1, 2, and 4 hours post injection (p.i.), and transferred to EDTA tubes for plasma generation, and frozen at −20°C. For analysis, 50 µL aliquots were mixed with 150 µL 2:9:9 10 mmol/L NH_4HCO_3/acetonitrile/methanol (containing an analytical internal standard) and centrifuged. Supernatants were quantitated for BCY-B2 by LC/MS-MS. Pharmacokinetic parameters were determined by noncompartmental analysis using the software package PK Solutions 2.0 from Summit Research Services.

Metabolites identification in *ex vivo* mouse plasma

0.5-, 1-, and 2-hour timepoint samples derived from the pharmacokinetic study with BCY-B2 were analyzed. All possible proteolytic metabolites and molecular weights of BCY-B2 were predicted based on endoproteolytic Loop 1 and/or Loop 2 opening leading to mass addition of 1 or 2x H_2O; and exoproteolytic removal of single AA's or AA stretches from either or both loops. Using an LTQ Orbitrap XL Mass Spectrometer, samples were extracted as above and scanned directly for proteolytic metabolites based on their predicted exact mass (10 ppm mass window). Signal intensities were recorded, compared with the signal intensity of the intact parent molecule, and classified into low, medium, and high intensity.

Cell culture

HT1080 and DU-145 cells [obtained from ATCC (CCL-121, HTB-81)] were cultured in EMEM medium enriched with 10% FCS and 2 mmol/L L-glutamine. MCF-7 cells [obtained from European Collection of Authenticated Cell Cultures (ECACC) (ECACC86012803)] and LNCaP (metastatic lesion of human prostatic adenocarcinoma, ATCC CRL-1740) were cultured in RPMI medium enriched with 10% FCS and 2 mmol/L L-glutamine (all from PAA, Etobicoke, Canada). Cells were grown at 37°C in humidified air with 5% CO_2 and were harvested using trypsin-ethylenediaminetetraacetic acid (trypsin-EDTA; 0.25% trypsin, 0.02% EDTA; Invitrogen). Cell line authentication and mycoplasma testing is regularly performed. The authentication of MT1-MMP-positive HT1080 cell line used for the *in vivo* experiments was confirmed on March 16, 2016. The authentication of MT1-MMP-negative LNCaP cell line was confirmed on July 03, 2018. The DU-145 cell line has been obtained from ATCC directly before the *in vivo* experiment was started (purchased on July 10, 2018; Lot: 2215512). Typically, less than 20 passages between thawing and use in the described experiments were done. Details on cell uptake and internalization experiments are provided in Supplementary Materials and Methods.

Radiolabeling with ^{177}Lu, ^{67}Ga, ^{68}Ga; mAb HBED-CC labeling

Radioisotope labeling with ^{177}Lu (organ distribution and internalization studies), ^{67}Ga (mAb organ distribution), and ^{68}Ga (PET studies) and HBED-CC labeling of the mAb was performed according to previously established protocols, detailed in Supplementary Materials and Methods.

Organ distribution and PET imaging

All experiments were conducted in accordance with the German Law on the care and use of laboratory animals, and the ARRIVE guidelines. The experiments were approved by the regional authorities *Regierungspräsidium Karlsruhe* (approval number G138/15) and *Regierungspräsidium Freiburg* (approval number G17-142). The mice were housed at constant temperature (room temperature) and relative humidity under regular light/dark schedule. Food and water were available *ad libitum*.

5×10^6 cells of HT1080, DU-145, or LNCaP, respectively, were subcutaneously inoculated into the right flank of male 6-week-old BALB/c nu/nu mice (Charles River Laboratories). Tumors were grown for ∼1 week, to ∼200 mm^3. Respective doses were prepared by mixing a fixed quantity of 5 pmoles ^{177}Lu-labeled peptides (at approx. 50 kBq) with different quantities of non-labeled peptide (derived from 1 mmol/L stock solution in 0.25 M sodium acetate pH 7 + 0.05% Tween20) in 100 µL injection buffer (0.25 M sodium acetate pH 7, 0.05% Tween20). For the anti-MT1-MMP mAb, 0.08–0.1 nmol ^{67}Ga-labeled HBED-CC-antibody (containing approx. 1 MBq activity) dissolved in 100 µL 0.9% NaCl was used per mouse. At least three animals were used per dose and timepoint. Radiolabeled peptide or antibody solutions were injected via the tail vein, followed by sacrifice at various time points. Organs of interest (blood, heart, lung, spleen, liver, kidney, muscle, small intestine, brain, HT1080 tumor, and femur) were dissected, blotted dry, and weighed. The radioactivity was measured using a gamma counter and calculated as %ID/g, and corrected for ^{67}Ga/^{177}Lu decay. µPET imaging for all cell lines in the xenograft models, autoradiography, and IHC detection of MT1-MMP in different tumor sections are described in Supplementary Materials and Methods.

Statistical aspects

Biodistribution experiments were performed at least in triplicate. Quantitative data were expressed as mean ± SD. If applicable, means were compared using Student *t* test. *P* values < 0.05 were considered statistically significant. Affinity data errors are reported as 95% confidence limits and used $n \geq 3$ for all key compounds, except some compounds prepared for the chemical optimization campaign.

Results

Identification of a high affinity bicyclic peptide targeting MT1-MMP

Using methodology previously described (5), bicyclic peptide phage libraries containing three cysteines with six randomized amino acids (AA) situated between Cys_i, Cys_{ii} (Loop 1) and Cys_{ii}, Cys_{iii} (Loop 2), respectively (6 × 6 format), were generated using 1,3,5-tris(bromomethyl)benzene as the thiol-reactive cyclization scaffold. Selections were performed to identify potent binders to the human hemopexin domain (PEX) of MT1-MMP. Bicyclic peptide BCY-A (sequence $C_iK_1N_2R_3G_4F_5G_6C_{ii}E_7D_8F_9Y_{10}$-$D_{11}I_{12}C_{iii}$) was abundantly present in sequence outputs. The K_d of its fluoresceinated version (BCY-A1) to PEX was 692 ± 66 nmol/L, as determined by fluorescence polarization (FP; Supplementary Table S2). Further selections using smaller sub-libraries based on BCY-A (randomized AA residues on positions 1–4, 5–8, and 9–12, respectively) were performed. Sequence outputs revealed similar sequences, with some in a 5 × 6 format. The sequence of the most abundant 5 × 6 output was $C_iY_1N_2E_3F_4G_5C_{ii}E_6D_7F_8Y_9$-$D_{10}I_{11}C_{iii}$ (BCY-B). Its fluoresceinated derivative (BCY-B1, C-terminally linked via a $sarcosine_6$ spacer to fluoresceinated lysine) showed strong affinity to PEX at $K_d = 1.1 \pm 0.4$ nmol/L (Supplementary Table S2), which is a nearly 630-fold improvement over the original BCY-A sequence. Moreover, the non-labeled, cysteine-terminated core bicyclic peptide (BCY-B2;

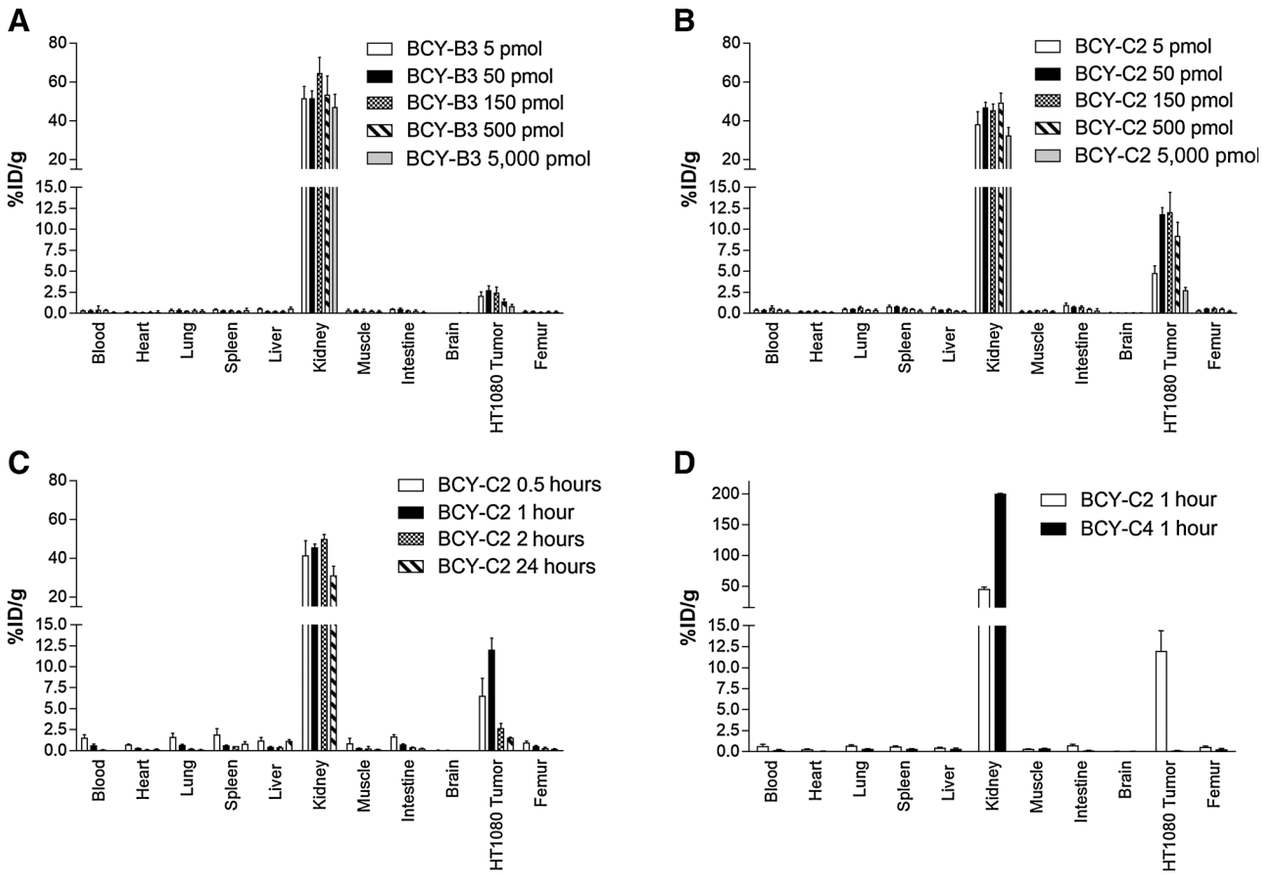

Figure 2.

Comparative organ distribution showing the dose range studies of the parental bicyclic peptide BCY-B3 (**A**) and the stability optimized variant BCY-C2 (**B**) at 1 hour p.i. using 5, 50, 150, 500, and 5,000 pmol peptide per mouse. **C,** Time-dependent organ distribution profile of BCY-C2 at the optimal dose (150 pmol/mouse) up to 24 hours p.i. **D,** Direct comparison of BCY-C2 to the nonbinding bis-Ala variant BCY-C4 at 1 hour p.i. at 150 pmol/mouse. Data are expressed as mean %ID/g tissue ± SD ($n = 3$).

Supplementary Table S2) retained its affinity to PEX ($K_d = 2.5 \pm 0.25$ nmol/L, as determined by FP competition), suggesting that the affinity is not impacted significantly by the presence of the fluorescent tag.

Internalization *in vitro* in MT1-MMP–expressing cell lines

The MT1-MMP overexpressing patient-derived fibrosarcoma cell line HT1080 (13) was selected to assess whether BCY-B recognizes endogenously expressed cell surface MT1-MMP. To this end, BCY-B was conjugated N-terminally to the chelator DOTA (1,4,7,10-tetraazacyclododecane-1,4,7,10-tetraacetic acid) to yield BCY-B3 (Fig. 1A; Supplementary Table S2) to facilitate complexation with imaging and therapeutic radionuclides. BCY-B3 retained its affinity to PEX ($K_d = 0.51 \pm 0.03$ nmol/L, with data confirmed by surface plasmon resonance; Supplementary Tables S2 and S3). Complexation of BCY-B3 with the γ- and β^- emitter ^{177}Lu at 98 °C was achieved readily, and radiochemical yields were >95% throughout. Incubation of ^{177}Lu-labeled BCY-B3 with HT1080 cells, alongside the nonexpressing cell line MCF-7 (14), showed cell surface binding as well as internalization in HT1080, but not in MCF-7 cells (Supplementary Fig. S1A). HT1080 cell incubation with BCY-B3 in the presence of an excess of nonradioactive peptide showed suppression of cell binding and uptake, confirming MT1-MMP–dependent binding and internalization (Supplementary Fig. S1B). Internalization of the peptide through receptor-mediated endocytosis (15) is desirable in the context of an imaging or targeting reagent, as it would lead to selective accumulation and prolonged retention in tumor cells.

BCY-B3 localizes to HT1080 xenograft tumors in mice

^{177}Lu-labeled BCY-B3 was then evaluated for its ability to target MT1-MMP *in vivo* using HT1080 xenograft tumor mice. A range of doses containing a fixed level of radiotracer (5 pmol at 50 kBq/mouse) were administered, organs and tumor excised 1 hour p.i., and measured for residual radioactivity. Significant tumor binding occurred at all doses (Fig. 2A; Supplementary Table S4), with the optimum residing at 150 pmol/mouse (~15 μg/kg, at 2.5 ± 0.67%ID/g). Excess cold BCY-B3 at the higher dose levels (500, 5000 pmol/mouse) reveals a strong suppression of the tumor signal, confirming that BCY-B3 tumor uptake is driven by saturable receptor binding and not an unspecific uptake mechanism. A strong kidney signal indicates renal clearance as a likely elimination mechanism. Remarkably, no other organ appears to be targeted by BCY-B. When assessing tumor uptake as a function of

time (150 pmol/mouse), BCY-B3 remains detectable in the tumor after 24 hours, with a maximum at the earliest time point at 0.5 hours p.i. consistent with rapid clearance of the peptide from the circulation (Supplementary Fig. S2A; Supplementary Table S5).

To demonstrate that BCY-B tumor localization is MT1-MMP–mediated and not nonspecific, we generated an inactive BCY-B3 variant, where every amino acid is substituted with its D-isomer (BCY-B4, $K_d \geq 10{,}000$ nmol/L; Supplementary Table S2). In a comparative xenograft study, BCY-B4 was not detectable in the tumor (Supplementary Fig. S2B; Supplementary Table S6), demonstrating MT1-MMP–dependent targeting.

Proteolytic metabolism of BCY-B *in vivo*

Given the peptidic nature of BCY-B, it is conceivable that abundant endogenous proteolytic activity in the blood stream, on epithelial surfaces and in the tumor microenvironment (16) could contribute to clearance *in vivo*, leading to suboptimal tumor targeting. *In vitro*, BCY-B had a half-life of nearly 11.5 hours in mouse plasma, and no measurable degradation in human plasma (Supplementary Table S1; Supplementary Fig. S3A and S3B). A mouse pharmacokinetic (PK) study using the minimal core bicyclic peptide BCY-B2 was performed. The peptide had an elimination half-life of 14 minutes, and is cleared at 20.7 mL/min/kg (Supplementary Fig. S4; Supplementary Table S7). The clearance rate is greater than the expected glomerular filtration rate (GFR) for hydrophilic molecules observed in mice (17), indicating additional nonrenal clearance mechanisms. Blood samples derived from the PK study were further analyzed by mass spectrometry for potential proteolytic degradation products of BCY-B2. Three metabolites could be identified unequivocally, having a 10% to 20% signal compared with parent. These top three metabolites corresponded to excision of $Y_1N_2E_3$, $Y_1N_2E_3F_4$, and $Y_1N_2E_3F_4G_5$ in Loop 1. Further traces at <2% compared with parent corresponded to degradation mostly in Loop 2 (loss of Y_1/Y_9, Y_9D_{10}, $D_7F_8Y_9/F_8Y_9D_{10}$, $Y_9D_{10}I_{11}$, $E_6D_7F_8Y_9D_{10}I_{11}$), and additional traces suggested simultaneous degradation in Loop 1 and 2. Thus, *in vivo* metabolites appear to center on initial endo-proteolytic cleavage at or near Tyr_1 and Tyr_9, followed by successive exo-proteolytic removal of residues in the vicinity, ultimately leading to potential removal of both loops in their entirety (Supplementary Fig. S5). Together, the measurable degradation in *in vitro* plasma, the *in vivo* clearance rate exceeding GFR, and the detection of distinct *in vivo* metabolites supports that BCY-B *in vivo* clearance is accelerated by proteolytic degradation.

Proteolytic stabilization of BCY-B

We undertook a campaign of chemical optimization to identify modifications enhancing the proteolytic stability. Eleven derivatives of BCY-B2 were generated where each AA was replaced by alanine (Table 1). Ala substitutions on positions 1, 3, 10, and 11 were mostly tolerated, with affinities dropping no more than five-fold, indicating a lesser role of these sidechains. The equipotent $Tyr_1 \rightarrow Ala_1$ substitution is of particular interest as it removes the Tyr_1 *in vivo* proteolytic recognition point. Because of the proteolytically stabilizing effect of D amino acids on amide bonds nearby (18), we next performed a partial D-alanine scan in Loop 1. $Tyr_1 \rightarrow$ D-Ala_1 binds at 10-fold lower affinity ($K_d = 24$ nmol/L). Interestingly, substitution of Gly_5 with D-Ala_5 (but not L-Ala_5) yields an equipotent molecule, presumably due to the unique torsion angles that glycine can adopt (Table 1; ref. 19). In Loop 2, potential proteolysis inhibiting homophenylalanine (HPhe) or phenylglycine (PhG) isosteric substitutions at Tyr_9 were associated with loss in affinity. Nearby Ile_{11} substitution with the *tert*-butylglycine modestly enhances affinity and protects the nearby amino acid backbone from proteolytic hydrolysis by steric obstruction (Table 1; ref. 18).

Table 1. L-Alanine, D-Alanine scan and isostere substitutions in BCY-B2

L-Alanine scan	K_d (nmol/L)
Parent compound BCY-B2	2.5 ± 0.25
$Tyr_1 \rightarrow Ala_1$	3.8
$Asn_2 \rightarrow Ala_2$	>5,000
$Glu_3 \rightarrow Ala_3$	5.1
$Phe_4 \rightarrow Ala_4$	34
$Gly_5 \rightarrow Ala_5$	>5,000
$Glu_6 \rightarrow Ala_6$	>5,000
$Asp_7 \rightarrow Ala_7$	>5,000
$Phe_8 \rightarrow Ala_8$	>5,000
$Tyr_9 \rightarrow Ala_9$	>5,000
$Asp_{10} \rightarrow Ala_{10}$	11.1
$Ile_{11} \rightarrow Ala_{11}$	8
D-Alanine scan	**K_d (nmol/L)**
$Tyr_1 \rightarrow$ D-Ala_1	24
$Asn_2 \rightarrow$ D-Ala_2	>5,000
$Glu_3 \rightarrow$ D-Ala_3	105
$Phe_4 \rightarrow$ D-Ala_4	>5,000
$Gly_5 \rightarrow$ D-Ala_5	2.4
Isostere substitutions	**K_d (nmol/L)**
$Phe_4 \rightarrow Tyr_4$	1.8 ± 0.45
$Phe_4 \rightarrow Trp_4$	0.75 ± 0.23
$Phe_4 \rightarrow HPhe_4$	43
$Phe_4 \rightarrow PhG_4$	628
$Phe_4 \rightarrow$ 3,4-DCPhe_4	1.9 ± 2.5
$Phe_4 \rightarrow 1NAl_4$	0.36 ± 0.12
$Phe_4 \rightarrow 2NAl_4$	0.7 ± 0.19
$Phe_4 \rightarrow Chg_4$	>5,000
$Phe_4 \rightarrow Cha_4$	362
$Phe_4 \rightarrow tBuGly_4$	>5,000
$Tyr_9 \rightarrow HPhe_9$	>5,000
$Tyr_9 \rightarrow PhG_9$	>5,000
$Ile_{11} \rightarrow tBuGly_{11}$	1.6 ± 1.1

NOTE: The sequence of BCY-B2 (Ac-$C_iY_1N_2E_3F_4G_5C_{ii}E_6D_7F_8Y_9D_{10}I_{11}C_{iii}$) was modified at the positions as indicated. Binding affinities were determined by FP competition.

Phage selection sequence outputs also indicated occurrence of aromatic amino acids Trp and Tyr at position 4 in Loop 1. The corresponding peptides showed enhanced affinity (3.3-fold for Trp) to PEX (Table 1). Moreover, upon incorporation of aromatic and non-aromatic isosteres of Phe/Tyr/Trp [e.g., homophenylalanine, phenylglycine, 3,4-dichlorophenylalanine (3,4-DCPhe4), 1- and 2-naphthylalanine (1NAl, 2NAl), and non-aromatic cyclohexylglycine (Chg), cyclohexylalanine (Cha), and *tert*-butylglycine (tBuGly)], 1-Naphthylalanine showed a strong seven-fold increase in affinity. The less tolerated modifications are non-aromatic (Chg, Cha, tBuGly) or present the incorrect distance between Cα and the aromatic group (HPhe, Phg; Table 1).

Finally, we synthesized a bicyclic peptide incorporating all protease-stabilizing modifications (D-Ala_1, D-Ala_5 and $tBuGly_{11}$) as well as the affinity-enhancing $Phe_4 \rightarrow 1NAl_4$ (BCY-C, sequence: C_i [D-Ala]$_1N_2E_3$ [1NAl]$_4$ [D-Ala]$_5C_{ii}E_6D_7F_8Y_9D_{10}$[tBuGly]$_{11}C_{iii}$). $Phe_4 \rightarrow 1NAl_4$ was included to counteract the affinity-reducing effects of $Tyr_1 \rightarrow$ D-Ala_1. Remarkably, all four modifications in concert are compatible and in fact improve the potency to MT1-MMP slightly (1.3 ± 0.7 nmol/L; BCY-C1 Supplementary Tables S1 and S2). Finally and importantly, compared with

BCY-B, BCY-C showed no measurable degradation in mouse and human plasma over the course of 24 hours (Supplementary Fig. S3A and S3B). This was equally confirmed for the radiolabeled derivative BCY-C2 (Fig. 1B; Supplementary Table S1). Moreover, both BCY-B3 and BCY-C2 exhibit modest blood plasma protein binding at <30%.

Cell internalization and selectivity of BCY-C

Compared with BCY-B, the DOTA derivative of BCY-C (Fig. 1B, BCY-C2, $K_d = 0.52 \pm 0.24$ nmol/L; Supplementary Tables S1 and S2) showed a 1.7- and 2.3-fold greater level of cell association and internalization, respectively, using HT1080 cells *in vitro*, demonstrating that its greater stability to proteases enhances cell binding and uptake. Binding and uptake could be efficiently blocked by an excess of non-labeled peptide, once again demonstrating specificity (Supplementary Fig. S1B). In confocal microscopy experiments, the Alexa Fluor 488-modified fluorescent BCY-C showed HT1080 plasma membrane and lysosomal localization following 30 minutes exposure at 500 nmol/L concentrations, whereas its nonbinding D-amino acid analogue did not, supporting selective receptor-driven internalization and trafficking to the lysosomal compartment (Supplementary Fig. S6; ref. 15).

Using a fluoresceinated derivative of BCY-C and FP, we could detect an equal affinity to both PEX and the whole extracellular ectodomain of MT1-MMP (wherein PEX is contained), but no measurable binding to the extracellular catalytic domain alone, demonstrating that BCY-C is specific for PEX and that the major protease function of MT1-MMP is not impeded (Supplementary Table S8). The selectivity was further assessed towards the most homologous human metalloproteinases MMP-1, MMP-2, MMP-15, and MMP-16 using FP. None of the metalloproteinases showed measurable binding at 1,000 nmol/L (Supplementary Table S8), indicating high selectivity of BCY-C for MT1-MMP. Moreover, BCY-C was fully cross-reactive with the mouse hemopexin domain (which differs only by one residue from human PEX). Collagen, an endogenous binding partner of PEX (20), was not competitive with BCY-C binding to PEX, showing that BCY-C binding does not disrupt this interaction.

Stabilized BCY-C improves tumor uptake *in vivo*

In the xenograft tumor mouse, BCY-C2 showed a striking 4.9-fold increase in tumor signal compared with nonstabilized BCY-B3 (150 pmol/mouse, 1 hour p.i.; Fig. 2B; Supplementary Table S9). The more delayed maximum tumor signal at 1 hour p.i. (compared with 0.5 hours for BCY-B3) in the corresponding time course study (Fig. 2C; Supplementary Table S10) plausibly stems from improved tumor exposure and accumulation due to the higher stability to proteases (Supplementary Table S1). To assess specificity, we generated an inactive variant of BCY-C2 containing two alanine replacements at positions 5 and 6 in the sequence. The choice of alanine replacement was based on the alanine scan

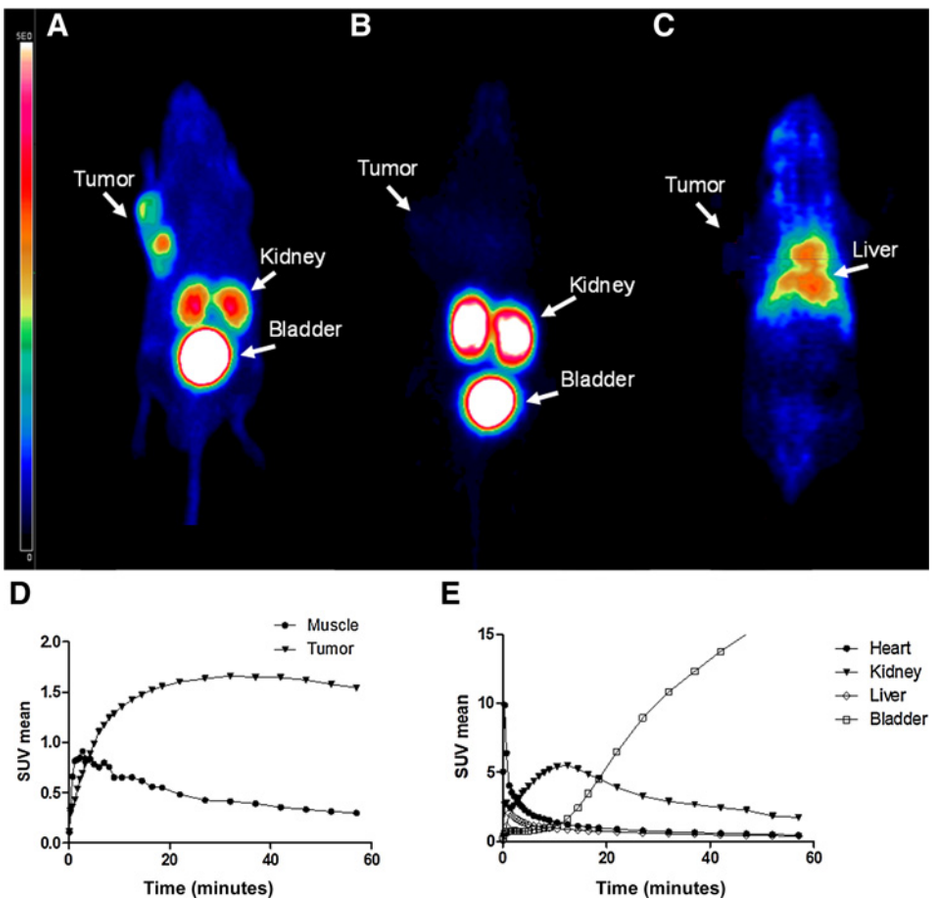

Figure 3.
PET imaging of BCY-C2, BCY-C4, and mAb in HT1080 xenograft mice. Whole-body maximum intensity projections were obtained 40 to 60 minutes p.i. from μPET imaging of ^{68}Ga-labeled stabilized BCY-C2 (**A**), ^{68}Ga-labeled inactive Ala_5/Ala_6 variant BCY-C4 (**B**), and ^{68}Ga-labeled MT1-MMP–specific mAb (**C**). Time activity curves using BCY-C2 are shown for tumor and muscle (**D**) and heart, kidney, liver, and bladder (**E**).

data in Table 1. The resultant derivative, BCY-C4, had no measurable binding to MT1-MMP up to 10,000 nmol/L (Supplementary Table S2). In the HT1080 xenograft mouse, BCY-C4 localization to the tumor could not be observed (Fig. 2D; Supplementary Table S11), again indicating MT1-MMP-dependent targeting for BCY-C2 *in vivo*.

μPET imaging of BCY-C2 and its inactive variant BCY-C4

In a follow-up μPET study using the ^{68}Ga-labeled derivative of BCY-C2, selective tumor uptake in the HT1080 xenograft model and rapid clearance from other organs resulting in high-imaging contrasts as early as 20 minutes post injection could be observed (Fig. 3A; Supplementary Fig. S7). By contrast, the nonbinding peptide BCY-C4 (Fig. 3B), as well as a PEX-specific mAb (Fig. 3C, refer also to paragraph "MT1-MMP targeting mAb shows reduced tumor accumulation") show no measurable uptake in the tumor or poor visualization, respectively. For BCY-C2, time activity curves indicate rapid clearance from muscle, liver, and heart; with the kidney signal peaking at 10 minutes and dropping thereafter, while the bladder continued to rapidly accumulate the radiolabeled peptide (Fig. 3D and E).

Comparative μPET imaging, autoradiography, and IHC

To further characterize the MT1-MMP-specific imaging properties of BCY-C2, a μPET imaging study comparing HT1080 with two other cell lines (DU-145, a medium expresser, and LNCaP, a non-expresser for MT1-MMP; refs. 21, 22) was performed. The data shows a robust correlation between the PET signal (Fig. 4A–C), the subsequent autoradiography of the resected tumors (Fig. 4D–F) and the expression levels on the tumors visualized by IHC using an antibody specific for MT1-MMP (Fig. 4G–I).

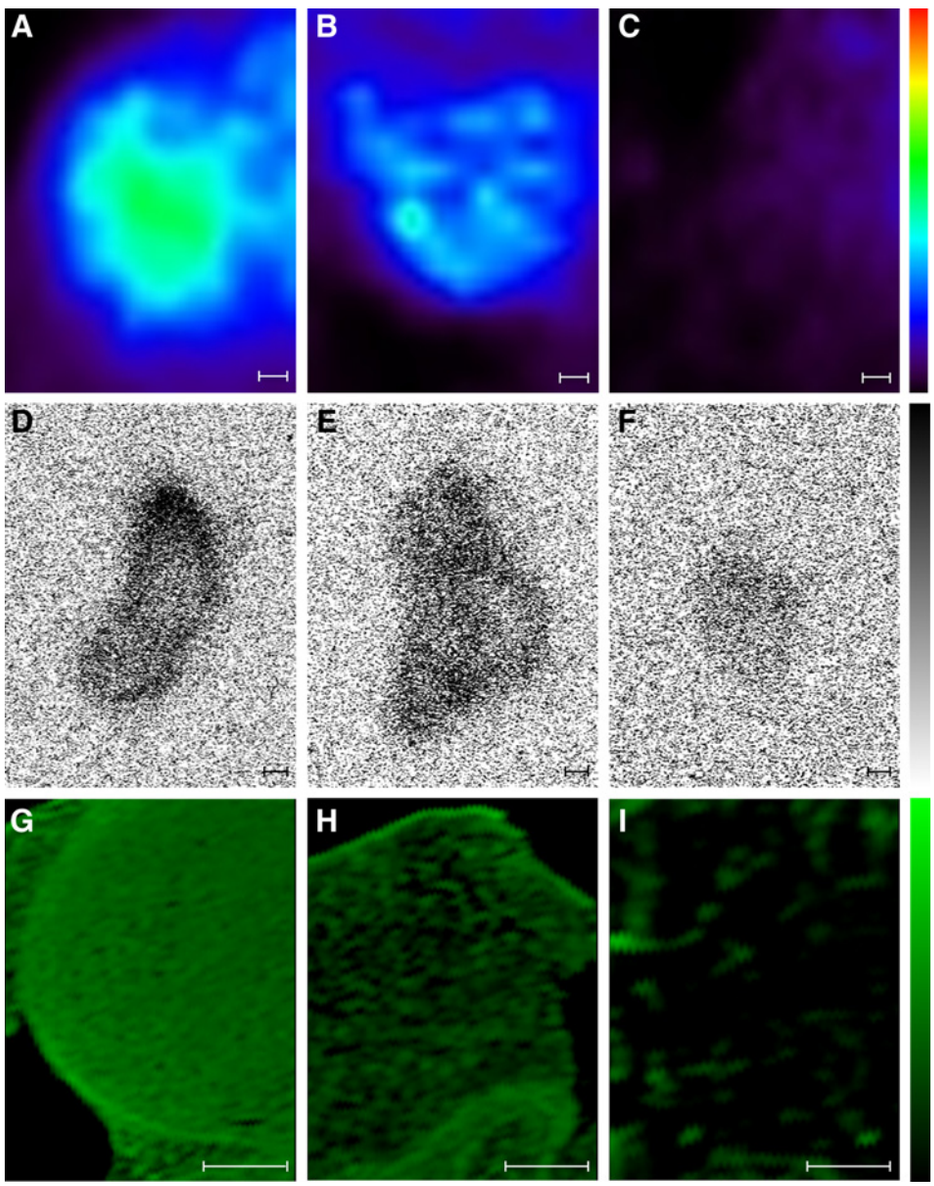

Figure 4.
Visualization of MT1-MMP expression with BCY-C2 in HT1080 (**A**, **D**, and **G**, high expression), DU-145 (**B**, **E**, and **H**, medium expression), and LNCaP (**C**, **F**, and **I**, MT1-MMP negative) xenograft mice. Maximum intensity projections of the tumors were obtained at 60 to 70 minutes p.i. by μPET imaging (**A–C**), followed by autoradiography studies of tumor cryosections, dissected after μPET imaging (**D–F**). IHC was performed with cryosections of a control group of mice with MT1-MMP mAb and NIR-detection (IRDye800CW conjugated goat-anti-mouse IgG; **G–I**). Scale bars, 1 mm.

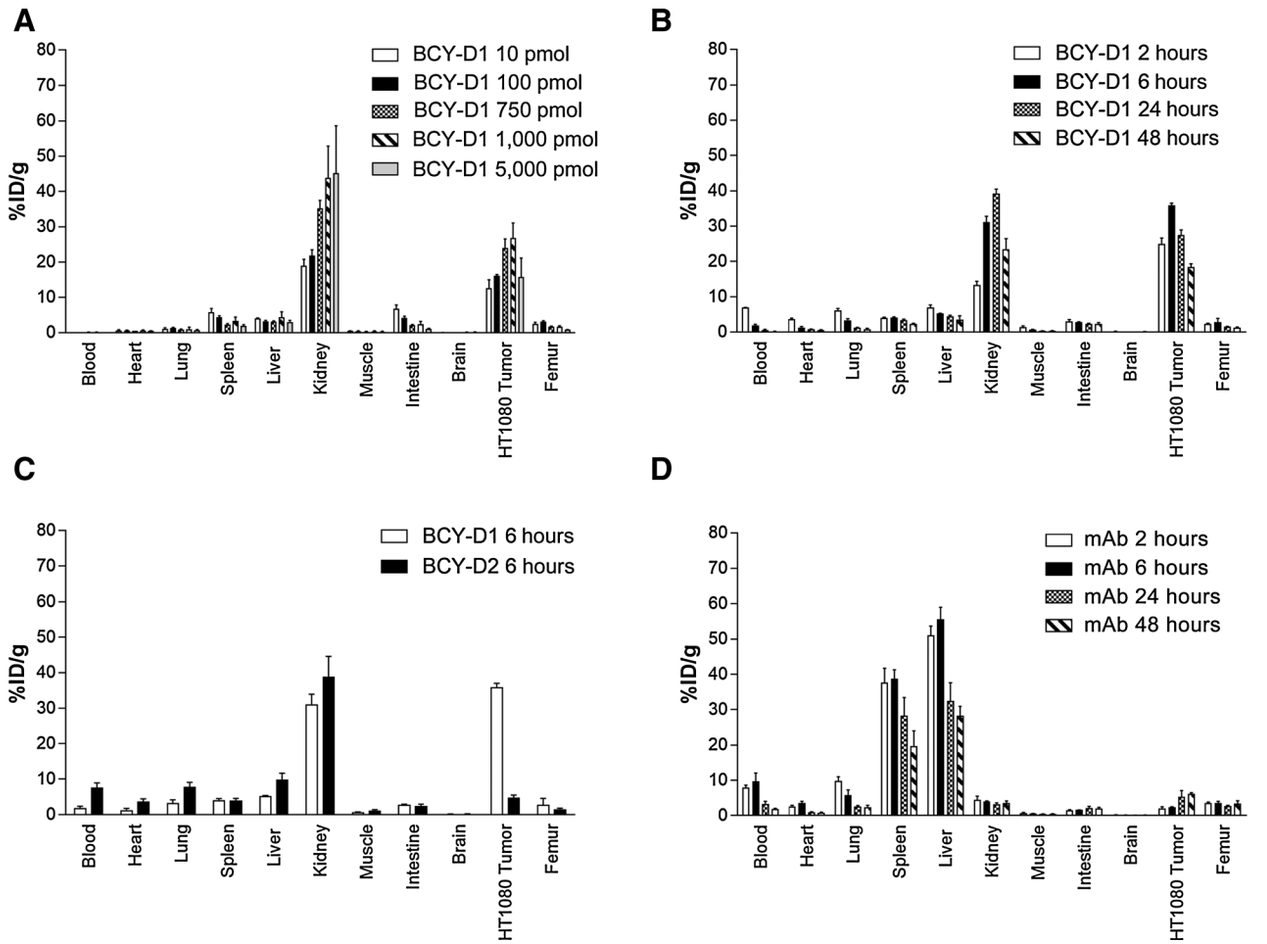

Figure 5.

Dose range and time course studies with palmitoylated BCY-D1 and inactive palmitoylated BCY-D2, and MT1-MMP–specific mAb. **A,** Organ distribution of BCY-D1 at a range of doses/mouse at 48 hours p.i. **B,** Time-resolved organ distribution of palmitoylated BCY-D1 at 750 pmol/mouse. **C,** Comparison of BCY-D1 with the nonbinding variant BCY-D2 at 6 hours p.i. at 750 pmol/mouse. **D,** Time-resolved organ distribution of MT1-MMP–specific mAb (90 pmol/mouse). Data are expressed as mean %ID/g tissue ± SD ($n = 3$).

Lipidated bicyclic peptide shows enhanced tumor uptake

Lipidation of biomolecules is known to increase serum half-life through serum albumin binding in the circulation (23), and could offer a potential modification to BCY-C to increase *in vivo* tumor binding and uptake through prolonged exposure. We generated a palmitoylated derivative of BCY-C, where its N-terminus was modified with an extended sarcosine$_{15}$ (Sar) oligomer spacer terminated with palmitoic acid, and where a lysine conjugated with DOTA was placed within the sarcosine spacer (BCY-D1, Fig. 1C). Oligosarcosine was chosen as a spacer for its extended, nonglobular structure, high aqueous solubility and proteolytic stability (24). BCY-D1 retained its affinity to MT1-MMP ($K_d = 2.3 \pm 0.85$ nmol/L; Supplementary Tables S2 and S3), and was fully soluble at $\geq$1 mg/mL in aqueous buffer (50 mmol/L Hepes, pH 7, 5% DMSO). Plasma protein binding studies with the radiolabeled peptide showed >99% in the bound fraction. A biodistribution study using ^{177}Lu-labeled BCY-D1 at varying doses was conducted and assessed at 48 hours p.i. (Fig. 5A; Supplementary Table S12). A high tumor signal of 24 ± 2.5%ID/g to 27 ± 4.3%ID/g was observed at the optimal dose of 750 to 1,000 pmol/mouse. Further signals at <4.5%ID/g were observed in spleen, liver, and small intestine. A subsequent organ distribution study investigating additional time points (2, 6, and 24 hours) at the optimal dose showed high tumor accumulation of 25 ± 1.6%ID/g as early as 2 hours p.i. (Fig. 5B; Supplementary Table S13). At 6 hours p.i., the tumor uptake of BCY-D1 reached an impressive maximum of 36 ± 1.1%ID/g, thereafter dropping slowly. To assess the *in vivo* specificity of BCY-D1, we generated Ala_5/Ala_6 nonbinder as before (BCY-D2). The organ distribution at 6 hours p.i. shows significantly reduced tumor uptake (4.8 ± 1.4%ID/g), which was in fact below the value observed in blood (7.7 ± 2.2%ID/g, Fig. 5C; Supplementary Table S14), indicating that the tumor signal of palmitoylated BCY-D1 is largely specific for MT1-MMP binding.

MT1-MMP targeting mAb shows reduced tumor accumulation

A comparative biodistribution study using a commercially available MT1-MMP-targeting mAb was performed. The affinity of the mAb, both when conjugated or not with the radiometal chelator HBED-CC, was at 3 nmol/L and thus comparable to the

peptides (Supplementary Methods). *In vivo*, the ^{67}Ga-labeled HBED-CC-mAb showed a distinctly different biodistribution profile to BCY-C2/BCY-D1, with the majority of radiolabeled mAb appearing in the spleen and liver (up to 60%ID/g) and lesser signals (between 2 and 10%ID/g) in the blood, heart, lung, kidney and femur (Fig. 5D; Supplementary Table S15). The xenograft tumor accumulated the radiolabeled mAb slowly, reaching its maximum at 48 hours p.i. (6.2%ID/g). A PET image generated using ^{68}Ga-labeled mAb (40–60 min p.i.) underlines its broad distribution into the major organs, with poor tumor visualization at this early time point (Fig. 3C).

Discussion

The identification and optimization of tumor-selective agents both for high-contrast molecular imaging and molecular targeting is driven by a variety of complex and intertwined factors. These range from choice of tumor-associated target antigen, binding affinity and selectivity to the target, *in vivo* stability and metabolic clearance, and importantly, accumulation in the target tissue with concomitant clearance from the circulation and nontarget organs. Further considerations concern extravasation and tumor penetration: diffusion rates into extravascular spaces decline steeply as a function of hydrodynamic volume; however, extended exposure ensues with increasing molecular size at molecular weights >60 kDa due to reduced clearance by renal filtration (25), counteracting the unfavorably slow penetration kinetics associated with larger molecular size. Theoretical and experimental work suggest maximal tumor uptake occurring for targeting agents the size of an antibody (~150 kDa) and for molecules at <5 to 10 kDa, whereby high affinities are critical for the latter to ensure maximal target engagement during first pass (26, 27). Monoclonal antibodies of high binding affinity can be readily identified to most extracellular targets, and thus have been extensively investigated in molecular imaging, at times serving as companion diagnostics to successful mAb-based molecular targeted anti-cancer drugs [e.g., trastuzamab (anti-Her2), rituximab (anti-CD20), bevacizumab (anti-VEGFA)]. Nonetheless, only a handful of mAb-based imaging agents have gained approval for clinical use. The slow kinetics in achieving optimal tumor to background signal ratios (2–4 days) in patients, necessitating matching long-lived radionuclides and therefore excluding a number of common radionuclides such as ^{18}F, ^{99m}Tc, or ^{68}Ga, has perhaps hampered development (28, 29).

Not surprisingly, other modalities, in particular peptides and small protein domains, have been investigated extensively, in part because of their small-size promising rapid tumor penetration and high signal to background ratios, greater flexibility regarding use of short-lived radionuclides, and chemical versatility that synthetic peptides in particular offer. A considerable range of often linear tumor-homing peptides is documented in the literature, with a subset demonstrating *in vivo* imaging (30, 31). However, to date the most prominent and effective examples of imaging peptides in clinical development or practice (e.g., somatostatin analogues) are derived from naturally occurring precedents often presented in a cyclic format, suggesting that the options available for the discovery and development of clinically attractive peptidic targeting agents remain limited (32, 33).

Here, we used bicyclic peptide libraries to identify potent tumor-homing agents. We anticipated that the constrained, bicyclic format should impart intrinsically favorable potency, specificity, and stability characteristics. Phage selections identified BCY-B, a 1.8 kDa acidic bicyclic peptide that showed impressive subnanomolar affinity to human and mouse MT1-MMP, and target-dependent binding and internalization in MT1-MMP$^+$ cells. *In vivo*, BCY-B rapidly and selectively accumulated in the tumor. However, mass spectrometry analysis of blood samples revealed proteolytic metabolism occurring *in vivo* at Tyr_1 and/or Tyr_9, plausibly accelerating *in vivo* clearance and concomitant reduction of tumor signal.

Table 2. Direct comparison of the tumor uptake values and T/B ratios of the nonstabilized bicyclic peptide BCY-B3, stability-optimized BCY-C2, and lipidated BCY-D1

Early time point p.i. optimal for imaging	%ID/g tumor	T/B ratio
BCY-B; nonstabilized, 1 hour p.i.	2.46 ± 0.67	5.6
BCY-B; nonstabilized, 24 hours p.i.	1.29 ± 0.15	129
BCY-C; stabilized, 1 hour p.i.	12.0 ± 2.4	18.2
BCY-C; stabilized, 24 hours p.i.	1.54 ± 0.06	25.7
Late time point p.i. optimal for therapy	**%ID/g tumor**	**T/B ratio**
BCY-D; palmitoylated, 2 hours p.i.	25.0 ± 1.7	3.6
BCY-D; palmitoylated, 6 hours p.i.	35.8 ± 1.1	18.7
BCY-D; palmitoylated, 24 hours p.i.	27.5 ± 1.5	50.9
BCY-D; palmitoylated, 48 hours p.i.	18.5 ± 0.9	97.2

NOTE: Data were derived from organ distribution studies at the optimal dose (150 pmol/mouse for BCY-B3, BCY-C2, and 750 pmol/mouse for BCY-D1; Supplementary Tables S5, S10, and S13). BCY-C shows favorably high tumor uptake and T/B ratio at 1 hour p.i., suitable for imaging approaches (underlined). By contrast, BCY-D is more suitable for radiotherapeutic approaches given the extended persistence in the tumor (6, 24, and 48 hours p.i.).

In the ensuing campaign of chemical optimization, proteolytically stabilizing (D-alanine$_{1/5}$, *tert*-butylglycine$_{11}$) and potency enhancing (1-naphthylalanine$_4$) modifications were successfully combined to generate BCY-C, a subnanomolar bicyclic peptide with no measurable instability in murine blood plasma ($t_{1/2}$ >>48 hours). *In vivo*, the tumor signal in the xenograft mouse model increased dramatically to 12%ID/g at 1 hour p.i., with a T/B ratio of 18 compared with 5.6 for BCY-B3 at its maximum at 1 hour, demonstrating the superior properties of this molecule (Table 2; Supplementary Table S10). In μPET studies, BCY-C2 showed high-specific tumor uptake and fast background clearance resulting in high-imaging contrast as early as 20 minutes p.i. The correlation of the μPET tumor signal with IHC staining of tumor cryosections unequivocally confirms that the tumor signal is driven by specific peptide binding to MT1-MMP and reflects the receptor expression level.

Importantly, most of the nontumor-associated bicyclic peptide rapidly cleared into the bladder, with a fraction retained in the kidneys, and no significant signal detected in other organs. Peptide uptake in the kidneys is a common phenomenon, and it is likely attributed to kidney-expressed amino acid transporters and organic anion/cation transporters transiently binding the peptide (34). Methods to reduce kidney signals have been evaluated (e.g., amino acid pre-infusion), and are successfully applied clinically in peptide receptor radionuclide therapy (PRRT; refs. 35, 36); a strategy that could potentially be applied in this instance. Overall, the comparison of BCY-B and BCY-C shows that high proteolytic stability of the targeting peptide is key to maximal delivery to the tumor *in vivo*.

With a half-life of ~25 minutes of BCY-C2 in the blood circulation (estimated from data in Fig. 2C) the compound shows ideal PK-properties for clinical PET-imaging at early time points post injection and to be combined with short-lived radionuclides

such as ^{68}Ga (half-life 67.7 minutes) or ^{18}F (half-life 110 minutes). For a potential therapeutic use, we questioned whether greater exposure through serum half-life extension of the bicyclic peptide would increase the tumor signal beyond 12%ID/g at later time points. A variety of half-life extending modifications of biotherapeutics have been described, ranging from conjugates with large polymers (e.g., PEGylation), proteins (e.g., albumin, Fab fragments), and fatty acids (37). The latter appeared particularly attractive for application with imaging peptides due to low molecular size, ease of chemical synthesis, and clinical validation with the success of long-acting lipidated insulins (insulin detemir, insulin degludec) and glucagon-like peptide-1 derivatives (liraglutide, semaglutide; refs. 38, 39). Fatty acid modified molecules bind serum albumin noncovalently, with only a small fraction present in the unbound state at equilibrium. To ensure that the albumin-bound fraction remains capable of simultaneous engagement with MT1-MMP on tumor cells, the design of BCY-D1 (Fig. 1C) incorporated an extended soluble sarcosine spacer between the albumin-binding palmitoic acid and the bicyclic peptide to spatially separate the two functions of the molecule. The biodistribution study of BCY-D1 (which was experimentally found to bind plasma proteins at >99%) revealed an extended half-life of nearly 2 hours in the mouse blood circulation (Fig. 5B), with a tumor uptake of 25%ID/g at the same timepoint, indicating rapid tumor uptake despite the more slowly extravasating 70 kDa albumin:BCY-D1 complex (66.5 + 3.7 kDa). Thus, BCY-D1 tumor uptake may also be driven by free BCY-D1. At 6 hours p.i., the tumor signal increased further to a maximal 36%ID/g, and T/B ratios ranged from 19-, 51-, and 97-fold at 6, 24, and 48 hours p.i. (Table 2). Comparison to the nonbinding control peptide BCY-D2 shows that tumor uptake is specific. Aside from expected clearance through the kidneys, signals are present in liver, spleen, and intestine (<4%ID/g at 24/48 hours, Fig. 5), indicating a fraction of the peptide clearing additionally through the hepatobiliary route consistent with albumin FcRn recycling taking place in the liver (40). Overall, evaluation of the bicyclic peptide as its fatty acid modified derivative showed surprisingly high and persistent targeted tumor uptake *in vivo*, making it attractive for the combination with readily available long-lived therapeutic radionuclides (such as ^{177}Lu; half-life 6.7 days) and potential endoradiotherapy. There is considerable scope in further optimization of the tumor signal and *in vivo* selectivity, through alterations in the molecular design regarding placement, composition, and size of the molecular spacer, and through the use of fatty acid derivatives with a range of affinities to albumin (41).

Comparison of the equipotent MT1-MMP targeting antibody to the bicyclic peptide or its fatty acid modified derivative demonstrates the starkly different biodistribution and tumor penetration kinetics of the different modalities. With a half-life of 14 hours in the blood (estimated from data at 6 hours onwards, Fig. 5D), the tumor signal slowly increased up to 48 hours p.i., indicating delayed penetration and uptake due to the large molecular size. The highest signal of 6.2%ID/g at 48 hours remains two-/six-fold lower than BCY-C2/BCY-D1 at their respective maximums, and the time required to reach this maximum is ≥48-fold greater for the antibody compared with the ∼70-fold smaller BCY-C2 (maximum at 1 hour p.i.). Moreover, the highest T/B ratio of 3.2 (48 hours p.i.) was modest, compared with 18 for BCY-C2 (1 hour) and 97 for BCY-D1 (48 hours; Table 2; Supplementary Tables S10, S13, and S15). High signals in liver and spleen, as well as some renal uptake, are in line with established clearance mechanisms for immunoglobulins (42).

Taking into account all *in vivo* data obtained in this study, BCY-C2 proved to be an optimal imaging agent, whereas the palmitoylated variant BCY-D1 is an attractive development candidate for endoradiotherapy (Table 2). Indeed, the MT1-MMP targeting bicyclic peptide BCY-C2 compares favorably to peptidic imaging probes in clinical development or practice. DOTA-TOC, a DOTA-modified derivative of the cyclic peptide octreotide targeting somatostatin receptor subtype 2, is widely used for clinical diagnosis and endoradiotherapy of neuroendocrine tumors. In preclinical work, DOTA-TOC showed a level as high as 15.2%ID/g in transduced C6 tumors (43), however only ∼3%ID/g in the patient-derived cell line IMR32 (44). For cyclic RGD peptides targeting the αvβ3 integrin receptor, the PET probe ^{18}F-AH111585 (also known as ^{18}F-Flucliclatide) is evaluated in several clinical studies, and shows up to 2.2%ID/g in the tumor depending on the cell line used in the xenograft model (45, 46). Superior molecules based on cyclic knottin peptides have been described (4.5%ID/g; ref. 47). Finally, the PSMA-targeting peptidomimetic probes [^{18}F]DCFPyL and [^{18}F]PSMA-1007 showed 16 and 8%ID/g in LNCaP xenograft models, respectively, and are being pursued further in clinical investigations (48, 49). Notably, as with BCY-C, all reported imaging probes are cleared renally, with the only nontumor signal present in the kidneys and bladder.

In conclusion, high affinity bicyclic peptides can be conveniently identified by phage display and offer a powerful platform for the development of novel tumor-targeting pharmaceuticals with the potential to address most clinically relevant extracellular targets of interest. The candidate molecules are highly amenable to modulation of pharmacokinetic properties through chemical modification, and show impressive properties for the potential use as clinical diagnostic imaging agents. The combination with clinically relevant therapeutic radionuclides or potent cytotoxins holds tremendous promise in molecular targeted therapy of cancer, an approach that is currently under development (50).

Disclosure of Potential Conflicts of Interest

K. Kopka is a consultant/advisory board member of Telix Pharmaceuticals. No potential conflicts of interest were disclosed by the other authors.

Authors' Contributions

Conception and design: M. Eder, C.L. Stace, E.H. Walker, G. Bennett, K. Kopka, D.P. Teufel

Development of methodology: M. Eder, U. Bauder-Wüst, A.-C. Baranski, C.L. Stace, E.H. Walker, E.H. Walker, G. Bennett, D.P. Teufel

Acquisition of data (provided animals, acquired and managed patients, provided facilities, etc.): M. Eder, S. Pavan, U. Bauder-Wüst, K. van Rietschoten, A.-C. Baranski, H. Harrison, S. Campbell, C.L. Stace, E.H. Walker, E.H. Walker, L. Chen, U. Schierbaum, K. Leotta, U. Haberkorn, D.P. Teufel

Analysis and interpretation of data (e.g., statistical analysis, biostatistics, computational analysis): M. Eder, U. Bauder-Wüst, A.-C. Baranski, H. Harrison, S. Campbell, C.L. Stace, E.H. Walker, G. Bennett, U. Schierbaum, K. Leotta, D.P. Teufel

Writing, review, and/or revision of the manuscript: M. Eder, A.-C. Baranski, G. Bennett, U. Haberkorn, K. Kopka, D.P. Teufel

Administrative, technical, or material support (i.e., reporting or organizing data, constructing databases): S. Pavan, U. Bauder-Wüst, G. Mudd, U. Haberkorn, D.P. Teufel

Study supervision: D.P. Teufel

Acknowledgments

All animal experiments complied with the current laws of the Federal Republic of Germany. The authors would like to thank Drs. Gillian Langford, Mike Rigby, and Mike Skynner for critical review of this publication, and Dr Julia Kristensson, Katarzyna Dzionek, and Melanie Boll for experimental support.

The costs of publication of this article were defrayed in part by the payment of page charges. This article must therefore be hereby marked *advertisement* in accordance with 18 U.S.C. Section 1734 solely to indicate this fact.

Received February 10, 2018; revised October 11, 2018; accepted December 26, 2018; published first January 3, 2019.

References

1. Bailly C, Clery PF, Faivre-Chauvet A, Bourgeois M, Guerard F, Haddad F, et al. Immuno-PET for clinical theranostic approaches. Int J Mol Sci 2016;18. doi: 10.3390/ijms18010057.
2. Padma VV. An overview of targeted cancer therapy. Biomedicine (Taipei) 2015;5:19. doi: 10.7603/s40681-015-0019-4.
3. Kraeber-Bodere F, Bailly C, Cherel M, Chatal JF. ImmunoPET to help stratify patients for targeted therapies and to improve drug development. Eur J Nucl Med Mol Imaging 2016;43:2166–8.
4. Van Heertum RL, Scarimbolo R, Ford R, Berdougo E, O'Neal M. Companion diagnostics and molecular imaging-enhanced approaches for oncology clinical trials. Drug Des Devel Ther 2015;9:5215–23.
5. Heinis C, Rutherford T, Freund S, Winter G. Phage-encoded combinatorial chemical libraries based on bicyclic peptides. Nat Chem Biol 2009;5: 502–7.
6. Middendorp SJ, Wilbs J, Quarroz C, Calzavarini S, Angelillo-Scherrer A, Heinis C. Peptide macrocycle inhibitor of coagulation factor XII with subnanomolar affinity and high target selectivity. J Med Chem 2017;60: 1151–8.
7. Baeriswyl V, Rapley H, Pollaro L, Stace C, Teufel D, Walker E, et al. Bicyclic peptides with optimized ring size inhibit human plasma kallikrein and its orthologues while sparing paralogous proteases. ChemMedChem 2012;7: 1173–6.
8. Angelini A, Cendron L, Chen S, Touati J, Winter G, Zanotti G, et al. Bicyclic peptide inhibitor reveals large contact interface with a protease target. ACS Chem Biol 2012;7:817–21.
9. Li Y, Cai G, Yuan S, Jun Y, Li N, Wang L, et al. The overexpression membrane type 1 matrix metalloproteinase is associated with the progression and prognosis in breast cancer. Am J Translat Res 2015;7:120–7.
10. Wang YZ, Wu KP, Wu AB, Yang ZC, Li JM, Mo YL, et al. MMP-14 overexpression correlates with poor prognosis in non-small cell lung cancer. Tumour Biol 2014;35:9815–21.
11. Peng CW, Wang LW, Fang M, Yang GF, Li Y, Pang DW. Combined features based on MT1-MMP expression, CD11b + immunocytes density and LNR predict clinical outcomes of gastric cancer. J Transl Med 2013;11:153.
12. Devy L, Huang L, Naa L, Yanamandra N, Pieters H, Frans N, et al. Selective inhibition of matrix metalloproteinase-14 blocks tumor growth, invasion, and angiogenesis. Cancer Res 2009;69:1517–26.
13. Rasheed S, Nelson-Rees WA, Toth EM, Arnstein P, Gardner MB. Characterization of a newly derived human sarcoma cell line (HT-1080). Cancer 1974;33:1027–33.
14. Giambernardi TA, Grant GM, Taylor GP, Hay RJ, Maher VM, McCormick JJ, et al. Overview of matrix metalloproteinase expression in cultured human cells. Matrix Biol 1998;16:483–96.
15. Osenkowski P, Toth M, Fridman R. Processing, shedding, and endocytosis of membrane type 1-matrix metalloproteinase (MT1-MMP). J Cell Physiol 2004;200:2–10.
16. Mason SD, Joyce JA. Proteolytic networks in cancer. Trends Cell Biol 2011; 21:228–37.
17. Qi Z, Whitt I, Mehta A, Jin J, Zhao M, Harris RC, et al. Serial determination of glomerular filtration rate in conscious mice using FITC-inulin clearance. Am J Physiol Renal Physiol 2004;286:F590–6.
18. Gentilucci L, De Marco R, Cerisoli L. Chemical modifications designed to improve peptide stability: incorporation of non-natural amino acids, pseudo-peptide bonds, and cyclization. Curr Pharm Des 2010;16: 3185–203.
19. Chen S, Gfeller D, Buth SA, Michielin O, Leiman PG, Heinis C. Improving binding affinity and stability of peptide ligands by substituting glycines with D-amino acids. Chembiochem 2013;14:1316–22.
20. Tam EM, Moore TR, Butler GS, Overall CM. Characterization of the distinct collagen binding, helicase and cleavage mechanisms of matrix metalloproteinase 2 and 14 (gelatinase A and MT1-MMP): the differential roles of the MMP hemopexin c domains and the MMP-2 fibronectin type II modules in collagen triple helicase activities. J Biol Chem 2004;279: 43336–44.
21. Bonfil RD, Dong Z, Trindade Filho JC, Sabbota A, Osenkowski P, Nabha S, et al. Prostate cancer-associated membrane type 1-matrix metalloproteinase: a pivotal role in bone response and intraosseous tumor growth. Am J Pathol 2007;170:2100–11.
22. Nagakawa O, Murakami K, Yamaura T, Fujiuchi Y, Murata J, Fuse H, et al. Expression of membrane-type 1 matrix metalloproteinase (MT1-MMP) on prostate cancer cell lines. Cancer Lett 2000;155:173–9.
23. Di L. Strategic approaches to optimizing peptide ADME properties. AAPS J 2015;17:134–43.
24. Teufel DP, Johnson CM, Lum JK, Neuweiler H. Backbone-driven collapse in unfolded protein chains. J Mol Biol 2011;409:250–62.
25. Christensen EI, Birn H, Storm T, Weyer K, Nielsen R. Endocytic receptors in the renal proximal tubule. Physiology (Bethesda) 2012; 27:223–36.
26. Wittrup KD, Thurber GM, Schmidt MM, Rhoden JJ. Practical theoretic guidance for the design of tumor-targeting agents. Methods Enzymol 2012; 503:255–68.
27. Thurber GM, Zajic SC, Wittrup KD. Theoretic criteria for antibody penetration into solid tumors and micrometastases. J Nucl Med 2007; 48:995–9.
28. Wu AM. Antibodies and antimatter: the resurgence of immuno-PET. J Nucl Med 2009;50:2–5.
29. Wright BD, Lapi SE. Designing the magic bullet? The advancement of immuno-PET into clinical use. J Nucl Med 2013;54:1171–4.
30. Brown KC. Peptidic tumor targeting agents: the road from phage display peptide selections to clinical applications. Curr Pharm Des 2010;16: 1040–54.
31. Liu R, Li X, Xiao W, Lam KS. Tumor-targeting peptides from combinatorial libraries. Adv Drug Deliv Rev 2017;110-111:13–37.
32. Lu L, Qi H, Zhu J, Sun WX, Zhang B, Tang CY, et al. Vascular-homing peptides for cancer therapy. Biomed Pharmacother 2017;92:187–95.
33. Lee S, Xie J, Chen X. Peptide-based probes for targeted molecular imaging. Biochemistry 2010;49:1364–76.
34. Roth M, Obaidat A, Hagenbuch B. OATPs, OATs and OCTs: the organic anion and cation transporters of the SLCO and SLC22A gene superfamilies. Br J Pharmacol 2012;165:1260–87.
35. Deutscher SL. Phage display in molecular imaging and diagnosis of cancer. Chem Rev 2010;110:3196–211.
36. Kwekkeboom DJ, Mueller-Brand J, Paganelli G, Anthony LB, Pauwels S, Kvols LK, et al. Overview of results of peptide receptor radionuclide therapy with 3 radiolabeled somatostatin analogs. J Nucl Med 2005;46: 62S–6S.
37. Kontermann RE. Half-life extended biotherapeutics. Expert Opin Biol Ther 2016;16:903–15.
38. Lorenz M, Evers A, Wagner M. Recent progress and future options in the development of GLP-1 receptor agonists for the treatment of diabesity. Bioorg Med Chem Lett 2013;23:4011–8.
39. Zaykov AN, Mayer JP, DiMarchi RD. Pursuit of a perfect insulin. Nat Rev Drug Discov 2016;15:425–39.
40. Kim J, Bronson CL, Hayton WL, Radmacher MD, Roopenian DC, Robinson JM, et al. Albumin turnover: FcRn-mediated recycling saves as much albumin from degradation as the liver produces. Am J Physiol Gastrointest Liver Physiol 2006;290:G352–60.
41. Zorzi A, Middendorp SJ, Wilbs J, Deyle K, Heinis C. Acylated heptapeptide binds albumin with high affinity and application as tag furnishes long-acting peptides. Nat Commun 2017;8:16092.
42. Wang W, Wang EQ, Balthasar JP. Monoclonal antibody pharmacokinetics and pharmacodynamics. Clin Pharmacol Ther 2008;84:548–58.

43. Zhang H, Moroz MA, Serganova I, Ku T, Huang R, Vider J, et al. Imaging expression of the human somatostatin receptor subtype-2 reporter gene with 68Ga-DOTATOC. J Nucl Med 2011;52:123–31.
44. Provost C, Prignon A, Cazes A, Combaret V, Delattre O, Janoueix-Lerosey I, et al. 68Ga-DOTATOC and FDG PET imaging of preclinical neuroblastoma models. Anticancer Res 2016;36:4459–66.
45. Morrison MS, Ricketts SA, Barnett J, Cuthbertson A, Tessier J, Wedge SR. Use of a novel Arg-Gly-Asp radioligand, 18F-AH111585, to determine changes in tumor vascularity after antitumor therapy. J Nucl Med 2009; 50:116–22.
46. Kenny LM, Coombes RC, Oulie I, Contractor KB, Miller M, Spinks TJ, et al. Phase I trial of the positron-emitting Arg-Gly-Asp (RGD) peptide radioligand 18F-AH111585 in breast cancer patients. J Nucl Med 2008;49: 879–86.
47. Kimura RH, Cheng Z, Gambhir SS, Cochran JR. Engineered knottin peptides: a new class of agents for imaging integrin expression in living subjects. Cancer Res 2009;69:2435–42.
48. Harada N, Kimura H, Onoe S, Watanabe H, Matsuoka D, Arimitsu K, et al. Synthesis and biologic evaluation of novel 18F-labeled probes targeting prostate-specific membrane antigen for PET of prostate cancer. J Nucl Med 2016;57:1978–84.
49. Cardinale J, Schafer M, Benesova M, Bauder-Wust U, Leotta K, Eder M, et al. Preclinical evaluation of (18)F-PSMA-1007, a new prostate-specific membrane antigen ligand for prostate cancer imaging. J Nucl Med 2017;58: 425–31.
50. Valeur E, Gueret SM, Adihou H, Gopalakrishnan R, Lemurell M, Waldmann H, et al. New modalities for challenging targets in drug discovery. Angew Chem Int Ed Engl 2017;56:10294–323.